HHS Public Access

Author manuscript

J Bone Miner Res. Author manuscript; available in PMC 2015 August 06.

Published in final edited form as:

J Bone Miner Res. 2005 December ; 20(12): 2124–2137. doi:10.1359/JBMR.050806.

Periosteal Progenitor Cell Fate in Segmental Cortical Bone Graft Transplantations: Implications for Functional Tissue Engineering

Xinping Zhang[1], **Chao Xie**[1], **Angela SP Lin**[2], **Hiromu Ito**[1], **Hani Awad**[1,3], **Jay R Lieberman**[4], **Paul T Rubery**[1], **Edward M Schwarz**[1], **Regis J O'Keefe**[1], and **Robert E Guldberg**[2]

[1]Department of Orthopaedics, University of Rochester Medical Center, Rochester, New York, USA

[2]George W. Woodruff School of Mechanical Engineering, Parker H. Petit Institute for Bioengineering and Bioscience, Georgia Institute of Technology, Atlanta, Georgia, USA

[3]Department of Biomedical Engineering, University of Rochester, Rochester, New York, USA

[4]Department of Orthopaedic Surgery, University of California, Los Angeles, California, USA

Abstract

A murine segmental femoral bone graft model was used to show the essential role of donor periosteal progenitor cells in bone graft healing. Transplantation of live bone graft harvested from Rosa 26A mice showed that ~70% of osteogenesis on the graft was attributed to the expansion and differentiation of donor periosteal progenitor cells. Furthermore, engraftment of BMP-2–producing bone marrow stromal cells on nonvital allografts showed marked increases in cortical graft incorporation and neovascularization, suggesting that gene-enhanced, tissue engineered functional periosteum may improve allograft incorporation and repair.

Introduction—The loss of cellular activity in a structural bone allograft markedly reduces its healing potential compared with a live autograft. To further understand the cellular mechanisms for structural bone graft healing and repair and to devise a therapeutic strategy aimed at enhancing the performance of allograft, we established a segmental femoral structural bone graft model in mice that permits qualitative and quantitative analyses of graft healing and neovascularization.

Materials and Methods—Using this segmental femoral bone graft model, we transplanted live isografts harvested from Rosa 26A mice that constitutively express β-galactosidase into their wildtype control mice. In an attempt to emulate the osteogenic and angiogenic properties of periosteum, we applied a cell-based, adenovirus-mediated gene therapy approach to engraft BMP-2–producing bone marrow stromal cells onto devitalized allografts.

Results—X-gal staining for donor cells allowed monitoring the progression of periosteal progenitor cell fate and showed that 70% of osteogenesis was attributed to cellular proliferation and differentiation of donor progenitor cells on the surface of the live bone graft. Quantitative μCT

Address reprint requests to: Xinping Zhang, MD, PhD, The Center for Musculoskeletal Research, University of Rochester Medical Center, 601 Elmwood Avenue, Rochester, NY 14642, USA, Xinping_Zhang@URMC.rochester.edu.

Dr Rubery is a founder, the director, and owns stock in LAGeT LLC. All other authors have no conflict of interest.

analyses showed a 3-fold increase in new bone callus formation and a 6.8-fold increase in neovascularization for BMP-2/stromal cell–treated allograft compared with control acellular allografts. Histologic analyses showed the key features of autograft healing in the BMP-2/stromal cell–treated allografts, including the formation of a mineralized bone callus completely bridging the segmental defects, abundant neovascularization, and extensive resorption of bone graft.

Conclusions—The marked improvement of healing in these cellularized allografts suggests a clinical strategy for engineering a functional periosteum to improve the osteogenic and angiogenic properties of processed allografts.

Keywords

allografts; isografts; autografts; periosteum; functional tissue engineering

INTRODUCTION

There is an increasing demand for bone grafts in orthopedic reconstructive surgeries. It is estimated that >500,000 bone-grafting procedures are performed annually in the United States; of these, about 55% are autografts, 35% are allografts, and about 10% are other materials.[1] Experimental and clinical studies have shown that fresh autogenous grafts produce superior incorporation and repair compared with allogeneic bone grafts. However, the use of devitalized bone allografts has continued to increase because of the ready availability of large structural allografts and the ability to avoid donor site morbidities associated with autografts.

Large structural bone allografts have excellent mechanical strength and are considered, by many, to be superior to currently approved synthetics or biopolymers. Some aspects of mechanical performance, such as fracture toughness, are particularly desirable.[2,3] No equivalent alternative to the use of large cadaveric allografts currently exists. Unfortunately, the loss of the cellular activity in a processed graft markedly reduces its healing potential compared with an autograft.[4–11] Furthermore, both remodeling and neovascularization of structural allografts are very poor because of the dense nature of the cortical bone. Retrieval studies of large human allografts show that revascularization of the graft penetrates no more than 8 mm deep from its surface.[12–14] The limited new bone formation and neovascularization of structural allografts are directly associated with the 25% clinical failure rate caused by fibrotic nonunions and late graft fractures.[15,16] Fractures in humans typically occur 1–2 years after surgical implantation and are related to propagating microfractures within the dead cortical bone.[17]

Bone graft healing is initiated by an inflammatory response and then followed by vascular invasion and recruitment of mesenchymal stem cells (MSCs), a process similar to fracture healing.[18] The later phase of graft repair and remodeling varies depending on whether the graft is composed of cortical or cancellous bone.[5–9] Cancellous bone graft is porous, revascularized quickly, and can be rapidly incorporated and remodeled. In this type of graft, osteoblastic bone formation occurs first on the surface of necrotic trabeculae followed by osteoclastic bone remodeling. This process gradually resorbs the entrapped dead trabeculae and eventually replaces the entire graft with new living bone. In contrast, vascularization of

cortical bone grafts is very slow and requires an initial phase of bone resorption. Thus, union of cortical grafts begins at the host–graft junction and gradually spreads toward the midshaft of the structural graft. The repair and remodeling of cortical bone occurs at a very slow rate, and any imbalance between resorption and bone formation can lead to bone loss and graft failure.[4–6,19]

It is known from clinical experience that preservation of the periosteum or use of a periosteal tube graft significantly improves bone graft incorporation and remodeling. There are also experimental data that support a critical role for live periosteal cells in cortical autograft healing.[15,20,21] We have previously shown in a murine segmental bone-grafting model that live autografts exhibited better incorporation and repair than devitalized allografts or bone isografts. Devitalized allografts completely relied on endochondral bone formation at the host–graft cortical junction, with absence of periosteal bone formation along the length of the graft. No differences in healing between processed isografts and allografts were found in this model, indicating that the host immune response does not significantly affect graft healing.[22]

The periosteum contains mesenchymal progenitor cells that are vital for endochondral and intramembraneous bone formation in cortical bone healing.[18,23–25] The two potential roles for periosteal cells are (1) proliferation and differentiation to form cartilage or new bone and/or (2) release of osteoinductive factors to recruit and activate osteoprogenitors from the host. The relative contribution of the two mechanisms to cortical bone healing currently is not clear. Establishing this information is critical to our understanding of the limits of allograft healing and the development of adjuvants to improve structural bone grafting.

To understand the complex cellular responses and interactions seen during healing of cortical bone grafts, we established a qualitative and quantitative method to examine bone graft healing and neovascularization in a segmental bone graft mice model using μCT. We performed cortical bone graft transplantation using live bone graft harvested from Rosa 26A mice,[26] which constitutively express β-galactosidase. Using X-gal staining of frozen sections, we were able to track the fate of periosteal mesenchymal cells in the course of cortical bone graft repair. Furthermore, to mimic the function of the periosteum, we engrafted isogeneic bone marrow stromal cells (BMSCs) modified using adenovirusmediated BMP-2 gene therapy onto devitalized bone allografts to induce an osteogenic and angiogenic response that closely resembles live autograft healing.

MATERIALS AND METHODS

Mouse strains

The breeding colonies of C57BL/6 mice and Rosa 26A mice were originally purchased from Jackson Laboratory. Allogeneic bone grafts were obtained from 129 mice for implantation into C57BL/6 mice. All animal surgery procedures were approved by University Committee of Animal Resources (UCAR).

Bone graft preparation and transplantation

Ten-week-old C57BL/6 mice were anesthetized by intraperitoneal injection with a combination of ketamine and xylazine. A 7- to 8-mm-long incision was made, and the midshaft femur was exposed by blunt dissection of muscles without disturbing the periosteum. A 4-mm mid-diaphyseal segment was removed from the femur by osteotomizing the bone using a saw. A 4-mm cortical bone graft was inserted into the segmental defect and stabilized by a 22-gauge metal pin placed through intramedullary marrow cavity, as previously described. The grafting procedures were performed between inbred C57BL/6 mice with identical genetic background (isograft) or mice with genetically different backgrounds (allograft). For live bone graft transplantation, the graft was carefully dissected out of muscles, briefly washed with warm PBS, and immediately transplanted into the mice (live isograft transplantation). To prepare live grafts free of periosteum and/or bone marrow, the graft surface was carefully scrapped to remove periosteum, and the marrow cavity was flushed with PBS to remove free bone marrow cells before transplantation. For devitalized bone graft transplantation, isografts from C57BL/6 mice or allografts from a genetically different strain were scrapped, extensively washed, sterilized with 70% ethanol, rinsed in saline to remove residual ethanol, and fresh frozen at −70°C for at least 1 week before transplantation. Graft healing was followed radiographically using a Faxitron X-ray system. The grafted femurs were also processed for histological and μCT analyses at the end time-point of the experiments. To monitor the periosteal cell fate, live grafts harvested from Rosa 26A mice were prepared without disturbing the periosteum and transplanted into congenic wildtype littermates. Mice were killed at 1, 3, 5, 7, 10, 14, 21, and 28 days after surgery and processed for cryosectioning.

Histochemical staining for β-gal and alkaline phosphatase

Fresh femur samples were fixed in 0.2% glutaraldehyde at 4°C for 4 days and washed twice in PBS for 15 minutes. All samples were decalcified in EDTA at 4°C for 14 days. After complete decalcification, samples were immersed in 30% sucrose at 4°C overnight and embedded in OCT compound (OCT) medium for cryosectioning. Consecutive tissue sections were refixed in 0.2% glutaraldehyde for 30 minutes, followed by two washes in PBS. All slides were stained in X-gal solution (0.02% NP40, 10 mM EDTA, 0.02% glutaraldehyde, 0.05% X-gal, and 2 mM $MgCl_2$ in phosphate buffer, pH 7.5) for 24 h. β-gal–positive cells were visualized and photographed under light microscopy. For alkaline phosphatase staining, tissue sections were rinsed in phosphate buffer three times and then washed in AP buffer (100 mM Tris-HCL, pH 9.5, 100 mM NaCl, 10 mM $MgCl_2$) for 10 minutes, followed by staining with substrates containing 0.2 mg/ml naphthol AS-MX phosphate and 0.4 mg/ml Fast red TR.

5-Bromo-2′-deoxyuridine labeling

5-Bromo-2′-deoxyuridine (BrdU) labeling solution (Zymed 00–0103) was injected into mice through the peritoneum at a dose of 10 ml/kg. Femurs were harvested 6 h after the injection and fixed in 0.2% glutaraldehyde as described previously. Immunohistochemical staining to detect BrdU+ cells were performed on frozen tissue sections according to the manufacturer's instructions (Zymed 00–0103) X-gal staining was performed before the staining for BrdU.

Histomorphometric analyses on bone and cartilage formation

After death, the grafted femurs were harvested, fixed in 10% neutral buffered formalin, and decalcified in 10% EDTA. At least three nonconsecutive 3-μm paraffinembedded sections were prepared and stained with Alcian blue/hematoxylin (H&E/Alcian blue).[27,28] Histomorphometric analysis was carried out using Osteometrics software to determine the area of periosteal new bone formation.[22] A line was drawn in the middle of the distal or proximal junctions between graft and host bone to separate new bone formation on the surface of the graft and the host bone. Areas of new bone formation on the side of the host or graft were measured separately at both ends to evaluate host and graft bone formation. To evaluate the cellular contribution from donor graft, three longitudinal tissue sections of the entire femur from each animal were analyzed by an investigator to determine the number of β-gal–positive chondrocytes, osteoblasts, and osteocytes from the host and donor in the healing graft tissue. Cell types were distinguished based on their distinctive morphology and location within the tissue. Because the expansion of donor stem cells covered large areas of blue-stained cartilage and new bone, we quantified the area of donor or host derived cartilage and new bone on the host side and donor side. The mean values from the three sections represented the value for one mouse.

BMSC culture and adenovirus infection

Bone marrow cells were isolated from 2-month-old C57BL/6 mice as described previously.[28] Briefly, femora and tibias were removed aseptically and dissected free of adherent soft tissue. The bone ends were cut, and bone marrow cells were flushed from the marrow cavity by injecting MEM slowly at one end of the bone using a sterile 21-gauge needle. The marrow suspension was dispersed gently by pipetting several times to obtain a single cell suspension. Bone marrow cells (1×10^7) were plated on 60-mm culture dishes and cultured in α-MEM containing 15% FBS (Hyclone Laboratories, Salt Lake City, UT, USA) for 5 days. The media were removed after 5 days, and fresh MEM with 15% FBS plus 50 μg/ml ascorbic acid and 5 mM β-glycerophosphate was added. The cells were cultured for an additional 5 days until confluent. Cells were trypsinized and directly used in transplantation.

For viral infection, adenovirus Ad-LacZ or Ad-BMP-2 was purified as described[29,30] and applied to BMSC cultures at 1000 MOI. About 30–50% infection efficiency was achieved in BMSC cultures (data not shown). After a 1-h incubation with the virus, cells were trypsinized and loaded on Gelfoam (Pharmacia-Upjohn) scaffolds. The gelfoam scaffolds were cut into 0.5 × 0.5-cm strips, soaked in the growth medium, and seeded with approximately 1×10^6 BMSCs. Cellularized scaffolds were wrapped around devitalized allografts and transplanted immediately into segmental defects, as described above. Allografts with acellular Gelfoam scaffolds were used as negative controls. Quantitative analyses of neovascularization and new bone formation by μCT imaging were performed at 4 and 9 weeks, respectively, after engraftment in three groups: allograft with scaffold only (allo-acellular), allograft with BMSCs infected with LacZ virus (allo-LacZ), and allograft with BMSCs infected with BMP-2–producing virus (allo-BMP2). To examine the effects of the cells alone, BMSCs were harvested from Rosa 26 mice and cultured as described

previously. About 5×10^6 noninfected BMSCs were seeded on Gelfoam scaffolds for implantation.

Quantification of new bone formation using μCT analysis

Bone volume analysis was performed by scanning the femurs in a μCT imaging system (eXplore; GE Health-Care). From the 2D slice images generated, an appropriate threshold was chosen for the bone voxels by visually matching thresholded areas to grayscale images. The threshold and the volume of interest (VOI) were kept constant throughout the analyses for each femur. To measure the new bone volume, contour lines were drawn in the 2D slice images to exclude the allograft and the old host cortical bone. New bone volume in a VOI covering the entire length of allograft and 1 mm of the host bone at both bone graft junctions was used to evaluate graft healing (Fig. 6E).

Quantification of vascularity using μCT analysis

Vascular networks at the cortical bone junction and around the bone allografts were examined using μCT analysis combined with perfusion of a lead chromate–based contrast agent.[31] Microfil MV-122 (Flowtech) contrast media, a radiopaque silicone rubber compound containing lead chromate, was perfused through the heart along with 4% paraformaldehyde. After perfusion, the grafted femur was removed and scanned using a μCT imaging system (Scanco Medical, Bassersdorf, Switzerland) at a voxel size of 10.5 μm to image bone and vasculature (Fig. 1F). The samples were subsequently decalcified using 10% EDTA solution. After complete decalcification, the samples were scanned again to image only vascularization at the defect region (Fig. 1G). By registering the 2D slices before and after decalcification, contour lines were drawn to define a VOI that only included the vasculature in or immediately adjacent to bone graft and its cortical bone junctions. The tomograms were globally thresholded based on X-ray attenuation and used to render 3D images of the vasculature in new bone callus (Fig. 1G, red vessels), excluding the vessels in the surrounding tissues (Fig. 1G, yellow vessels). Histomorphometric analysis based on direct distance transform methods[32,33] was subsequently performed on the 3D images to quantify parameters of vascular network morphology, including vasculature volume (Vasc. Vol.), vessel thickness (Vess.Th), vessel density (Vess. Den.: defined as an average number of vessels intersected by test lines passing through the 3D image normalized by test line length), vessel spacing (Vess. Sp.), and degree of anisotropy.[31,34] Based on some of our preliminary data from radiographic analysis, neovascularization peaked at 3–4 weeks after transplantation; therefore, samples harvested at these timepoints were used in the analysis of neovascularization.

Statistical analysis

Data are expressed as mean ± SE. Statistical significance between experimental groups was determined by one-way ANOVA. A p value <0.05 was considered statistically significant.

RESULTS

Removal of live periosteum leads to poor graft incorporation in live isograft bone transplantation

To show the essential role of periosteum in structural bone graft healing, we removed periosteum or bone marrow cells from live bone isografts and compared their healing with intact live isograft transplantation or devitalized bone isograft transplantation. Radiological and histologic analyses were conducted at 14 days after surgery. Live bone isograft healing was characterized by an abundant new bone formation at host–graft junctions and along the shaft of the graft (Fig. 1A). A similar response was found in isograft transplantation after the removal of only bone marrow cells (Fig. 1B). In sharp contrast, a marked decrease in bone cartilaginous callus formation was found in isograft transplantation after the removal of periosteum from the graft (Fig. 1C). In these grafts, endochondral bone healing at the junction was largely dependent on osteogenic activity of the host, similar to devitalized bone isograft transplantation (Fig. 1D). Instead of new bone or cartilage formation on the graft surface, a fibrotic tissue was formed on the surface of the isograft, disrupting cortical bone graft union (Fig. 1C). Histomorphometric analysis showed a 63% decrease in new bone and cartilage formation in the group lacking periosteum compared with live isograft transplantation or live isograft transplantation with the removal of bone marrow only (Fig. 1E; $n = 4$).

Preservation of periosteum in live bone graft transplantation leads to marked induction of neovascularization

Neovascularization were further examined at 3 weeks after surgery in live bone isografts versus devitalized bone isografts using established μCT methods.[31] As shown in Figs. 1F–1J, neovascularization was limited to both junctions in the devitalized isograft (Fig. 1H), whereas robust angiogenesis was induced throughout in the live isograft (Fig. 1I). Total vessel volume was increased by 10-fold in live isograft compared with devitalized controls. Although the average thickness of the vessels was not different, vessel density was increased 2-fold, and average vessel separation was reduced by 50% in the live isografts. Degree of anisotropy, which shows the orientation of vessel distribution, was also decreased significantly in live isografts (Fig. 1J; $n = 4$).

Periosteal progenitor cell fate and cellular contribution to cortical bone healing

To further characterize the fate of donor periosteal progenitor cells and their contribution to cortical bone healing, live bone isografts from Rosa 26A mice were grafted to their wildtype littermates. Live Rosa 26A isografts in wildtype recipients produced the same robust periosteal bone formation (Fig. 2) as previously described. Endochondral bone formation was primarily observed at the cortical bone junctions, whereas intramembraneous bone formation was found along the midshaft potion of the graft.

X-gal staining of tissue sections revealed the temporal progression of periosteal progenitor cell fate during cortical bone graft healing. At day 1, periosteal cells on the donor graft surface, osteocytes within the cortex of the graft, and the cells within bone marrow space were positive for β-gal (Figs. 2B1 and 2D1). Cellular condensations consisting of only donor

β-gal–positive cells were observed on the surface of the donor graft at days 3, 5, and 7 (Figs. 2D2–2D4). These donor-derived progenitor cells further differentiated by day 10 to form cartilage or bone, consisting of chondrocytes, osteoblasts, and osteocytes positively stained for β-gal (Figs. 2D5 and 3H). At day 14, chondrocyte calcification, matrix degradation, and vascular invasion were evident (Figs. 2A6, 2B6, 2C6, and 2D6). Various cells, including chondrocytes, osteoblasts, and osteocytes, on the donor side of the graft stained positive for β-gal (Fig. 2D6). In contrast, cells located on the host side were largely negative for β-gal. By day 28, donor-induced cartilage matrix and new woven bone were resorbed or remodeled by the host, the bone callus was invaded by host bone marrow, and only a few cells within the new bone callus stained positive for β-gal (Figs. 2A7, 2B7, 2C7, and 2D7).

The proliferation and differentiation of donor periosteal progenitor cells were further examined using double staining for β-gal and BrdU labeling or alkaline phosphatase, respectively (Fig. 3). At day 1, a single layer of β-gal–positive cells that were weakly stained for alkaline phosphatase was detected on the surface of donor bone graft (Fig. 3A). By days 3 and 5, β-gal–positive alkaline phosphatase negative periosteal mesenchymal cells formed cellular condensations on the graft surface at the interface with host bone (Figs. 3B and 3C). Most of these same cells were also positive for BrdU labeling (Fig. 3D). At day 7, hypertrophic chondrocytes were found highly positive for alkaline phosphatase staining, whereas a large proportion of β-gal–positive mesenchymal cells remained alkaline phosphatase low or negative (Fig. 3E, #). At day 10, β-gal–positive mesenchymal progenitor cells were completely replaced by β-gal–positive, alkaline phosphatase–positive hypertrophic chondrocytes (Fig. 3F).

In addition to endochondral bone formation at the cortical bone junctions, periosteal cells from the donor initiated features of intramembranous bone formation at the midshaft of the graft, which were evident by days 7 (Fig. 3G) and 10 (Fig. 3H). In these areas, alkaline phosphatase was strongly expressed (Figs. 3G and 3H, #), and finely trabeculated structures were formed among cellular condensations (Fig. 2A5). By day 10, new woven bone was formed, which contained a majority of β-gal–positive osteocytes (Fig. 3H, arrows). In addition to osteocytes, donorderived osteoblasts (Fig. 3I) and vessel-lining cells (Fig. 3K) were also observed in this area.

Histomorphometric analyses were performed to quantify the cellular contribution of donor periosteal progenitor cells to the remodeling and incorporation of bone grafts over a time period of 28 days (Fig. 4). On either the donor side (Fig. 4A) or the host side (Fig. 4B), cartilage formation peaked at day 10, whereas new bone formation culminated on day 21, suggesting graft healing in this murine model primarily proceeded through endochondral bone formation. It is also evident that donor periosteal cells only contributed a small percentage of osteogenic cells participating in bone formation on the host side of the graft junction (Fig. 4B). Interestingly, however, donor progenitor cells were the primary initiators of early cartilage and new bone formation on the graft side. Donor cell contribution peaked at day 10, when 73 ± 15% area of cartilaginous tissue and 70% new woven bone on the graft side were found to be positive for β-gal. After day 10, host-dependent remodeling of cartilage and new bone led to rapid replacement of donor tissues and cells, such that by day 28, few osteoblasts or osteocytes were positive for β-gal (Fig. 4A).

Endosteum/marrow cell contribution to the osseointegration at the cortical bone junction was also examined. Although in a few samples harvested on day 21, we observed some β-gal–positive donor-derived chondrocytes and osteocytes localized within the marrow space on the side of graft, insertion of the intramedullary metal pin for fixation clearly destroyed most of the bone marrow tissue within the graft's intramedullary canal. In fact, H&E staining indicated that most of the identifiable donor bone marrow cells were dead (Fig. 2). As such, this model does not allow quantitative analysis of the contribution of endosteal cells to graft repair.

BMSC engraftment markedly improves bone allograft healing

To endow the allograft with an engineered functional periosteum, osteogenic BMSCs infected with BMP-2 (allo-BMP2) or control LacZ (allo-LacZ) adenovirus were seeded on Gelfoam scaffolds and engrafted onto devitalized bone allograft before transplantation into syngeneic mice. Four weeks after grafting, a marked increase in neovascularization was shown at both cortical bone junctions and along the bone allografts in animals receiving the allo-BMP2 grafts (Figs. 5A–5C). Quantitative analysis of vascular networks (Figs. 5D–5G) showed that, in the allo-BMP2 grafts, total vessel volume and vessel density increased by 6.8-fold (Fig. 5D; $p < 0.01$, $n = 4$), and 25% (Fig. 5F; $p < 0.01$), respectively, whereas vessel separation decreased by 29% (Fig. 5E; $p < 0.01$) compared with allo-LacZ control grafts. In addition, the degree of vessel anisotropy in the allo-BMP2 grafts decreased by 17% (Fig. 5H; $p < 0.01$), indicating a less oriented and more isotropic vessel network was generated. Vessel thickness remained unchanged among the three groups analyzed (Fig. 5G; $p > 0.05$). No significant differences in vascularity were detected between allo-LacZ grafts and allografts wrapped with acellular scaffolds (allo-acellular).

New bone formation was further evaluated using μCT imaging of the grafted femurs 9 weeks after transplantation. Marked induction of new bone callus formation was observed in the allo-BMP2 grafts (Figs. 6C and 6D) compared with the allo-acellular grafts (Fig. 6A). 3D reconstruction of the allo-BMP2 grafted femur showed solid bridging between the distal and proximal ends of the allograft by new bone callus (Figs. 6C and 6D), resembling healing in live isograft transplantation (Figs. 6E and 6F). Quantitative analysis showed a 3-fold increase in new bone formation in the allo-BMP2 grafts compared with acellular allografts (Fig. 6H; $n = 4$, $p < 0.05$), whereas only a small increase in bone formation was noted in the allo-LacZ grafts compared with acellular controls, which did not reach statistical significance.

In comparison with live isograft transplantations, radiographic and μCT analyses showed that a bridging bone callus formed across the allo-BMP2 grafts at around 4 weeks after grafting, similar to that observed in the timecourse of osteogenesis in live isograft healing (Figs. 6M and 6O). In these samples, new bone was found to integrate into the host bone and the allograft bone (Fig. 6M). By 13 weeks, the new bone callus completely surrounded the allograft (Fig. 6N). However, there were marked differences in the resorption of the live isografts and allografts. The live isografts underwent rapid resorption and remodeling such that, by 13 weeks, an estimated 60–70% of the graft was resorbed, leaving the bridging new bone callus as the major weight-bearing structure for the grafted femur (Fig. 6P). In contrast,

resorption and remodeling of the allografts were very slow. In control allo-acellular grafts, limited resorption was only observed at the cortical bone junctions 13 weeks after grafting, which led to bone loss at the junction in some cases (Fig. 6J, arrow). In contrast, although resorption and remodeling of the allo-BMP2 graft was much slower than the live isograft, significant induction of graft resorption and remodeling were observed throughout the devitalized allograft between 9 and 13 weeks after implantation (Fig. 6N, arrow).

Histological analysis confirmed the μCT results. In the allo-BMP2 grafts, newly formed bone callus was shown to encase the dead bone allografts, similar to that observed in the isograft transplantation groups. By 13 weeks, the scaffold was completely resorbed, and new bone callus was invaded by bone marrow cells (Fig. 7C). TRACP staining showed extensive osteoclastic bone resorption of the grafts (Fig. 7F). In the control allo-acellular graft, limited new bone formation was shown at the junction, with fibrous tissue disrupting the healing (Fig. 7A). In this group, osteoclastic resorption of the allograft seemed to originate from the invasive fibrous tissue (Fig. 7D). Although we did not observe significant quantifiable improvements in the allo-LacZ grafts, histologically these grafts appeared to exhibit better qualitative incorporation into the host bone than the allo-acellular grafts (Fig. 7B).

To determine if the lack of osteogenesis observed in the grafts encased with MSCs without BMP-2 transfection could be overcome by using more progenitors, we performed the experiments using Gelfoam scaffolds seeded with five times the number of uninfected cells derived from Rosa 26A mice. This increase in cellularity led to significant induction of osteogenesis, albeit poorly organized, around the allograft (Fig. 8A), with the new bone volume measuring 5.04 mm^3, which was greater than the callus volume in the allo-LacZ grafts but less than the allo-BMP2 grafts. X-gal staining showed blue osteocytes embedded in the new bone, in close proximity to the dead allograft 5 weeks after the surgery (Fig. 8C). Furthermore, the donor-derived osteocytes were found in new bone that formed on top of the dead allograft bone (Fig. 8C, arrow). TRACP staining showed active resorption and remodeling of the newly formed bone callus (Fig. 8D).

DISCUSSION

Using a mouse segmental femoral bone graft transplantation model, we showed that superior healing and repair of live isografts were attributed to the osteogenic and angiogenic activity of periosteum. Transplantation of Rosa 26A mice bone graft further revealed the significant cellular contribution of donor periosteal progenitor cells to cortical bone graft integration and remodeling. In an attempt to create a functional periosteum to improve devitalized bone graft healing, we combined tissue engineering and BMP-2 gene therapy strategies to engraft osteogenic BMSCs on the surface of the allograft. Both μCT and histological analyses showed that bone allografts wrapped with BMP-2–transfected stromal cells healed in a similar fashion to live isograft, as evidenced by marked formation of bridging new bone callus, extensive neovascularization, and bone graft resorption and remodeling.

The essential role of the periosteum in cortical bone healing has been extensively documented. However, our study is the first to mark the early mesenchymal progenitor cell population from periosteum using Rosa 26A mice and show that the expansion of these cells

accounted for 70% of endochondral and intramembraneous bone formation on the graft. These cells not only directly participated in chondrogenesis and osteogenesis, but also differentiated to form blood vessel lining cells and were directly involved in early angiogenesis. Although osteoinductive factors released from donor mesenchymal cells may induce bone formation through recruitment of host progenitors, our study showed that direct activation of the local periosteal progenitor cells is necessary and sufficient to induce an early healing response. The activation of these periosteal cells induced robust osteogenesis, accompanied by marked induction of angiogenesis. The initiation of early chondrogenesis and osteogenesis on the donor grafts is essential for host cell invasion, which eventually leads to vascularization and remodeling of bone graft. Histochemical staining further characterized these early periosteal donor cells as alkaline phosphatase negative (immature) but BrdU positive (rapidly dividing). The rapid proliferation of periosteal progenitor cells followed by differentiation to the osteoblast or chondroblast lineage support the paradigm that multiple transit progenitor populations exist, and the self-renewal or expansion of these cells could dramatically affect the outcome of healing and repair.[35,36]

Endochondral bone healing has been considered as a recapitulation of early fetal skeletogenesis.[37–39] Although many factors and genes involved in the two processes overlap, the initiation of the bone formation cascade by hematoma formation and early inflammatory response in the bone healing is absent in fetal bone development. Molecular and cellular mechanisms that control adult progenitor cell activation, expansion, and differentiation in the context of injury and repair are only superficially understood, mainly because of the lack of proper cellular markers for molecular analysis. Taking advantage of transgenic mouse models, this study presents a novel approach for marking and examining molecular regulation of the adult progenitor cell pool by growth factors and cytokines produced within local injury milieus.

Devitalized bone allografts have been widely used for reconstruction of large structural bone defects. Massive allografts can restore the size and shape of the resected bone. However, because of the lack of living cells and poor vascular supply, large structural bone allografting is associated with a high incidence of infection, nonunion, excessive resorption, and late fractures. The only effective intervention to save the failing structural allograft is to implant a vascularized graft in juxtaposition to allograft.[12,13,40] The success of this practice indicates the absolute requirement of a viable vascular network to bring active progenitor cells in close proximity to the devitalized bone graft.

The prolific osteogenic and angiogenic response by the periosteum in live bone isograft healing suggests that the presence of sufficient number of active progenitor cells in close proximity to bone grafts is essential for efficient graft healing and repair. To the end of engineering a functional periosteum for devitalized bone allograft, we engrafted BMSCs onto devitalized allograft and further used stromal cell–based BMP-2 gene therapy to recruit active stem cells from the nearby soft tissue. Our results showed four key features of live autograft healing that were realized in devitalized bone allografts implanted with BMP-2–producing BMSCs: (1) formation of a bridging and weight-bearing new bone callus across the whole length of dead allograft bone; (2) marked induction of angiogenesis within the new bone callus; (3) invasion of bone marrow cells within new bone callus; and (4) the

induction of extensive resorption and remodeling of the graft. The marked improvements in healing of cell-sheathed allografts further highlight the role of a vital periosteum and suggest future tissue engineering approaches for revitalization of processed structural bone allografts.

In these experiments, although direct induction of new bone formation on allografts implanted with BMP-2–producing BMSCs was observed, the efficiency of bone formation in the milieu of the allograft was less than that of the live isograft. This is likely because of the poor survival and differentiation of the progenitor cells within the bulky Gelfoam. Optimization of cell seeding density, scaffold thickness, and the engraftment protocol will be necessary to further enhance the integration and performance of these cellular allografts. The residual presence of the gelfoam and the less than efficient bone formation close to the allograft may also hinder the resorption and remodeling of the allografts compared with live isograft. Thinner scaffolds with higher resorption rates may allow more efficient vascular perfusion and marrow cell invasion, thereby facilitating the resorption and remodeling of the allograft. In addition, the lack of resorption and remodeling signals on the devitalized bone may also contribute to its poor integration and remodeling.[41] A recent report showed that osteocytes express RANKL in their dendritic processes; therefore, they could support osteoclast differentiation and survival in live bone graft.[42]

Our data showed that, under the same conditions (cell number, culture condition, viral particle), allografts implanted with BMP-2–producing stromal cells were vastly superior to noncellular allografts or allografts implanted with LacZ-transfected stromal cells. The seemingly ineffectiveness of the stromal cells transduced with LacZ virus could be caused by insufficient number of stromal cells initially loaded on the graft or the greater variability observed in this group of transplants. In fact, in a limited number of animals in which we increased the number of noninfected cells, we found that there were increased new bone formation around the allograft and better incorporation compared with LacZ controls. However, even with the increased cellularity, implantation of stromal cells alone was not sufficient to induce solid bridging and integration between cortical bone junctions, as observed in the live isografts or the allografts implanted with BMP-2–producing stromal cells (Fig. 8). It has been well documented that in stromal cell–based adenovirus-mediated BMP-2 gene therapy, the therapeutic effects of the genetically engineered mesenchymal cells were largely attributed to the paracrine function of BMP-2 produced by the cells.[43,44] It is also noteworthy to mention that Ad-LacZ–transduced stromal cells alone have not been sufficient to repair critical size defects or induce spine fusion as shown in several similar reports.[45,46] Further experiments are underway to optimize parameters influencing the engraftment of a functional periosteum, including the number of cells and the type and properties of the scaffold delivery vehicle.

In summary, our data show the critical cellular and molecular contributions of the periosteum to cortical bone repair. Furthermore, our data suggest that adult stem cell–based and gene-enhanced tissue engineering may offer novel and exciting therapeutic approaches to augment bone allograft healing and repair. With a focus on an osteogenic and angiogenic gene therapy, future efforts will be devoted to recapitulating all features of bone autograft healing and to inducing cell-mediated incorporation and remodeling of nonvital allografts.

This work could ultimately lead to new clinical strategies for functional revitalization and revascularization of large structural allografts.

ACKNOWLEDGMENTS

XZ is supported by The Orthopedic Research Education Foundation and Musculoskeletal Transplant Foundation and The National Institute of Health (AR051469). PR is supported by The Orthopedic Research Education Foundation and Musculoskeletal Transplant Foundation. RG is supported by NSF (EEC-9731643) and NIH (AR051336). ES is supported by grants from The Musculoskeletal Transplant Foundation and the NIH (AR45971). RO is supported by the NIH (AR46545). We also thank Loralee Gehan and Krista Canary for assistance with histological work.

REFERENCES

1. New materials for bone growth and tissue engineering. Med Pro. 1997; 7:135–140.
2. Davy DT. Biomechanical issues in bone transplantation. Orthop Clin North Am. 1999; 30:553–563. [PubMed: 10471760]
3. Tencer, A.; Johnson, K. Biomechanics in Orthopaedic Trauma. Philadelphia, PA, USA: JB Lippincott; 1994.
4. Burchardt H, Enneking WF. Transplantation of bone. Surg Clin North Am. 1978; 58:403–427. [PubMed: 349741]
5. Burchardt H. Biology of bone transplantation. Orthop Clin North Am. 1987; 18:187–196. [PubMed: 3550571]
6. Burchardt H. The biology of bone graft repair. Clin Orthop. 1983; 174:28–42. [PubMed: 6339139]
7. Garbuz DS, Masri BA, Czitrom AA. Biology of allografting. Orthop Clin North Am. 1998; 29:199–204. [PubMed: 9553565]
8. Goldberg VM, Stevenson S. The biology of bone grafts. Semin Arthroplasty. 1993; 4:58–63. [PubMed: 10148544]
9. Stevenson S. Biology of bone grafts. Orthop Clin North Am. 1999; 30:543–552. [PubMed: 10471759]
10. Stevenson S, Emery SE, Goldberg VM. Factors affecting bone graft incorporation. Clin Orthop. 1996; 324:66–74. [PubMed: 8595779]
11. Stevenson S, Li XQ, Davy DT, Klein L, Goldberg VM. Critical biological determinants of incorporation of nonvascularized cortical bone grafts. Quantification of a complex process and structure. J Bone Joint Surg Am. 1997; 79:1–16. [PubMed: 9010181]
12. Enneking WF, Mindell ER. Observations on massive retrieved human allografts. J Bone Joint Surg Am. 1991; 73:1123–1142. [PubMed: 1890115]
13. Enneking WF, Campanacci DA. Retrieved human allografts: A clinicopathological study. J Bone Joint Surg Am. 2001; 83:971–986. [PubMed: 11451965]
14. Tomford WW, Mankin HJ. Bone banking. Update on methods and materials. Orthop Clin North Am. 1999; 30:565–570. [PubMed: 10471761]
15. Berrey BH Jr, Lord CF, Gebhardt MC, Mankin HJ. Fractures of allografts. Frequency, treatment, and end-results. J Bone Joint Surg Am. 1990; 72:825–833. [PubMed: 2365716]
16. Lord CF, Gebhardt MC, Tomford WW, Mankin HJ. Infection in bone allografts. Incidence, nature, and treatment. J Bone Joint Surg Am. 1988; 70:369–376. [PubMed: 3279038]
17. Wheeler DL, Haynie JL, Berrey H, Scarborough M, Enneking W. Biomechanical evaluation of retrieved massive allografts: Preliminary results. Biomed Sci Instrum. 2001; 37:251–256. [PubMed: 11347398]
18. Einhorn TA. The cell and molecular biology of fracture healing. Clin Orthop. 1998; 355(Suppl):S7–S21. [PubMed: 9917622]
19. Bauer TW, Muschler GF. Bone graft materials. An overview of the basic science. Clin Orthop. 2000; 371:10–27. [PubMed: 10693546]

20. Liu JY, Wang D, Cheng HH. Use of revascularized periosteal allografts for repairing bony defects: An experimental study. Microsurgery. 1994; 15:93–97. [PubMed: 8183118]
21. Karaoglu S, Baktir A, Kabak S, Arasi H. Experimental repair of segmental bone defects in rabbits by demineralized allograft covered by free autogenous periosteum. Injury. 2002; 33:679–683. [PubMed: 12213418]
22. Tiyapatanaputi P, Rubery PT, Carmouche J, Schwarz EM, O'Keefe RJ, Zhang X. A novel murine segmental femoral graft model. J Orthop Res. 2004; 22:1254–1260. [PubMed: 15475206]
23. Szczesny G. Molecular aspects of bone healing and remodeling. Pol J Pathol. 2002; 53:145–153. [PubMed: 12476617]
24. Wlodarski KH. Normal and heterotopic periosteum. Clin Orthop. 1989; 241:265–277. [PubMed: 2647335]
25. Hutmacher DW, Sittinger M. Periosteal cells in bone tissue engineering. Tissue Eng. 2003; 9(Suppl 1):S45–S64. [PubMed: 14511470]
26. Zambrowicz BP, Imamoto A, Fiering S, Herzenberg LA, Kerr WG, Soriano P. Disruption of overlapping transcripts in the ROSA beta geo 26 gene trap strain leads to widespread expression of beta-galactosidase in mouse embryos and hematopoietic cells. Proc Natl Acad Sci USA. 1997; 94:3789–3794. [PubMed: 9108056]
27. Childs LM, Ulrich-Vinther M, Abuzzahab F, Zhang X, Xing L, Dougall W, Anderson D, Schwarz EM. Effects of RANK blockade on fracture healing. J. Orthoped Res. 2001; 21:676–684.
28. Zhang X, Schwarz EM, Young DA, Puzas JE, Rosier RN, O'Keefe RJ. Cyclooxygenase-2 regulates mesenchymal cell differentiation into the osteoblast lineage and is critically involved in bone repair. J Clin Invest. 2002; 109:1405–1415. [PubMed: 12045254]
29. Li P, Sanz I, O'Keefe RJ, Schwarz EM. NF-kappaB regulates VCAM-1 expression on fibroblast-like synoviocytes. J Immunol. 2000; 164:5990–5997. [PubMed: 10820282]
30. Lieberman JR, Daluiski A, Stevenson S, Wu L, McAllister P, Lee YP, Kabo JM, Finerman GA, Berk AJ, Witte ON. The effect of regional gene therapy with bone morphogenetic protein-2-producing bone-marrow cells on the repair of segmental femoral defects in rats. J Bone Joint Surg Am. 1999; 81:905–917. [PubMed: 10428121]
31. Duvall CL, Robert Taylor W, Weiss D, Guldberg RE. Quantitative microcomputed tomography analysis of collateral vessel development after ischemic injury. Am J Physiol Heart Circ Physiol. 2004; 287:H302–H310. [PubMed: 15016633]
32. Hildebrand T, Laib A, Muller R, Dequeker J, Ruegsegger P. Direct three-dimensional morphometric analysis of human cancellous bone: Microstructural data from spine, femur, iliac crest, and calcaneus. J Bone Miner Res. 1999; 14:1167–1174. [PubMed: 10404017]
33. Hildebrand T, Ruegsegger P. Quantification of bone microarchitecture with the structure model index. Comput Methods Biomech Biomed Engin. 1997; 1:15–23. [PubMed: 11264794]
34. Guldberg RE, Ballock RT, Boyan BD, Duvall CL, Lin AS, Nagaraja S, Oest M, Phillips J, Porter BD, Robertson G, Taylor WR. Analyzing bone, blood vessels, and biomaterials with microcomputed tomography. IEEE Eng Med Biol Mag. 2003; 22:77–83. [PubMed: 14699940]
35. Muschler GF, Midura RJ, Nakamoto C. Practical modeling concepts for connective tissue stem cell and progenitor compartment kinetics. J Biomed Biotechnol. 2003; 2003:170–193. [PubMed: 12975533]
36. Aubin JE. Advances in the osteoblast lineage. Biochem Cell Biol. 1998; 76:899–910. [PubMed: 10392704]
37. Ferguson C, Alpern E, Miclau T, Helms JA. Does adult fracture repair recapitulate embryonic skeletal formation? Mech Dev. 1999; 87:57–66. [PubMed: 10495271]
38. Ferguson CM, Miclau T, Hu D, Alpern E, Helms JA. Common molecular pathways in skeletal morphogenesis and repair. Ann NY Acad Sci. 1998; 857:33–42. [PubMed: 9917830]
39. Vortkamp A, Pathi S, Peretti GM, Caruso EM, Zaleske DJ, Tabin CJ. Recapitulation of signals regulating embryonic bone formation during postnatal growth and in fracture repair. Mech Dev. 1998; 71:65–76. [PubMed: 9507067]
40. Manfrini M, Vanel D, De Paolis M, Malaguti C, Innocenti M, Ceruso M, Capanna R, Mercuri M. Imaging of vascularized fibula autograft placed inside a massive allograft in reconstruction of lower limb bone tumors. AJR Am J Roentgenol. 2004; 182:963–970. [PubMed: 15039172]

41. Ito H, Koefoed M, Tiyapatanaputi P, Gromov K, Goater JJ, Carmouche J, Zhang X, Rubery PT, Rabinowitz J, Samulski RJ, Nakamura T, Soballe K, O'Keefe RJ, Boyce BF, Schwarz EM. Remodeling of cortical bone allografts mediated by adherent rAAV-RANKL and VEGF gene therapy. Nat Med. 2005; 11:291–297. [PubMed: 15711561]

42. Zhao S, Zhang YK, Harris S, Ahuja SS, Bonewald LF. MLO-Y4 osteocyte-like cells support osteoclast formation and activation. J Bone Miner Res. 2002; 17:2068–2079. [PubMed: 12412815]

43. Moutsatsos IK, Turgeman G, Zhou S, Kurkalli BG, Pelled G, Tzur L, Kelley P, Stumm N, Mi S, Muller R, Zilberman Y, Gazit D. Exogenously regulated stem cell-mediated gene therapy for bone regeneration. Mol Ther. 2001; 3:449–461. [PubMed: 11319905]

44. Turgeman G, Pittman DD, Muller R, Kurkalli BG, Zhou S, Pelled G, Peyser A, Zilberman Y, Moutsatsos IK, Gazit D. Engineered human mesenchymal stem cells: A novel platform for skeletal cell mediated gene therapy. J Gene Med. 2001; 3:240–251. [PubMed: 11437329]

45. Wang JC, Kanim LE, Yoo S, Campbell PA, Berk AJ, Lieberman JR. Effect of regional gene therapy with bone morphogenetic protein-2-producing bone marrow cells on spinal fusion in rats. J Bone Joint Surg Am. 2003; 85:905–911. [PubMed: 12728043]

46. Chang SC, Chuang HL, Chen YR, Chen JK, Chung HY, Lu YL, Lin HY, Tai CL, Lou J. Ex vivo gene therapy in autologous bone marrow stromal stem cells for tissueengineered maxillofacial bone regeneration. Gene Ther. 2003; 10:2013–2019. [PubMed: 14566360]

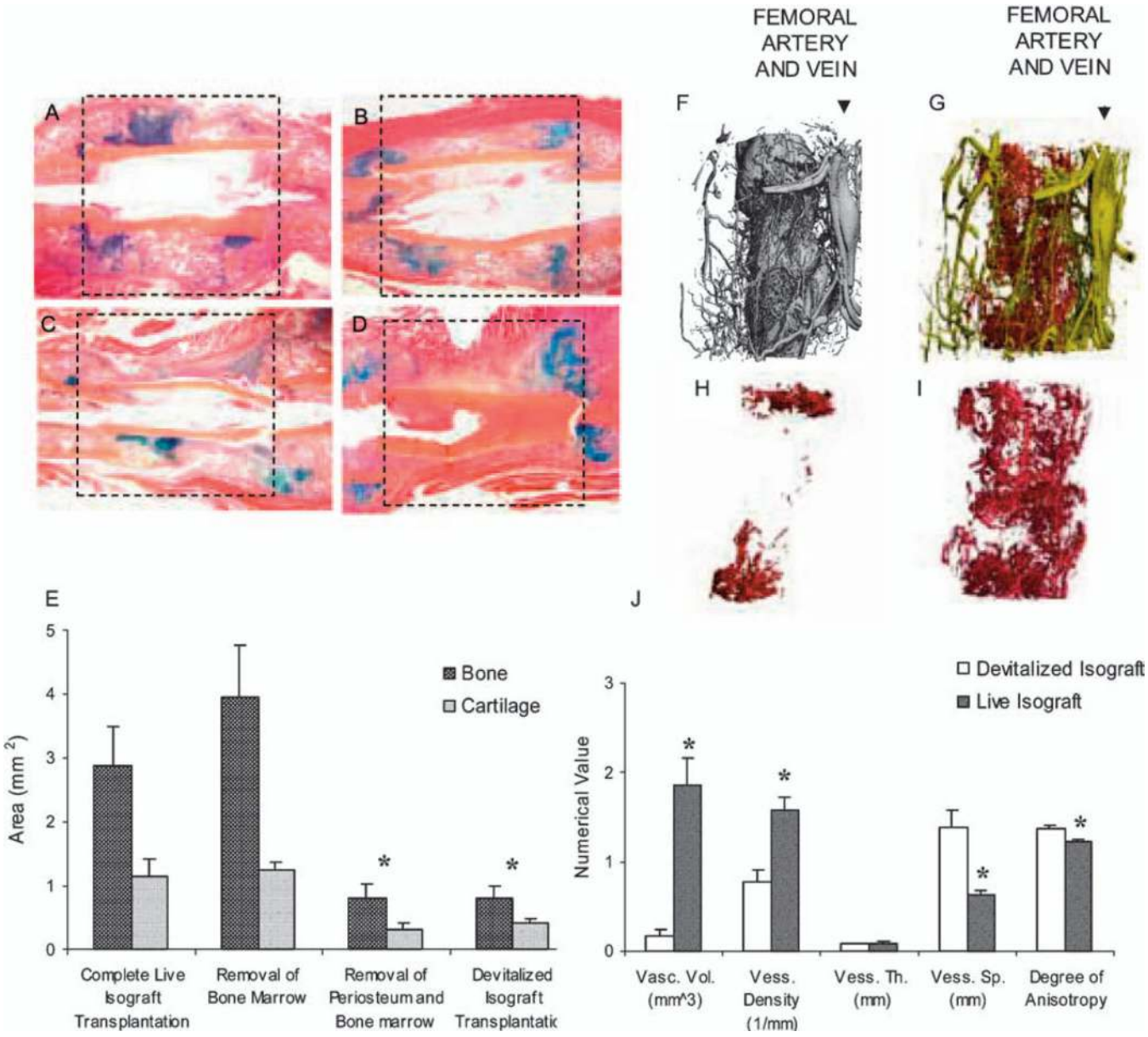

FIG. 1.

Live cortical bone graft healing and repair is mediated by periosteum. Representative Alcian blue/hematoxylin sections were obtained from grafted femurs 14 days after surgery. Extensive new bone formation across the bone graft is shown in the (A) intact live bone isograft or (B) the marrow-free live isograft. In contrast, a significant decrease in new bone callus formation is observed in (C) the periosteum-free bone isograft and (D) the devitalized bone isograft. (E) Histomorphometric measurements of bone callus formation around the bone graft (boxed region) are shown. *$p < 0.05$, $n = 4$. Experimental mice were perfused with Microfil 3 weeks after surgery. Grafted femurs were imaged using μCT (F) before decalcification and (G) after decalcification. The vessel networks in new bone callus are shown as red, whereas the vessel networks in soft tissue are shown as yellow. Representative 3D vascular images show vessel networks in (H) a devitalized isograft and

(I) a live isograft. (J) Quantitative volumetric and morphometric analyses on total vascular volume (Vasc. Vol.), vessel density (Vess. Den.), vessel separation (Vess. Sp.), vessel thickness (Vess. Th.) and degree of anisotropy. Data shown are mean ± SE. *$p < 0.05$, $n = 4$.

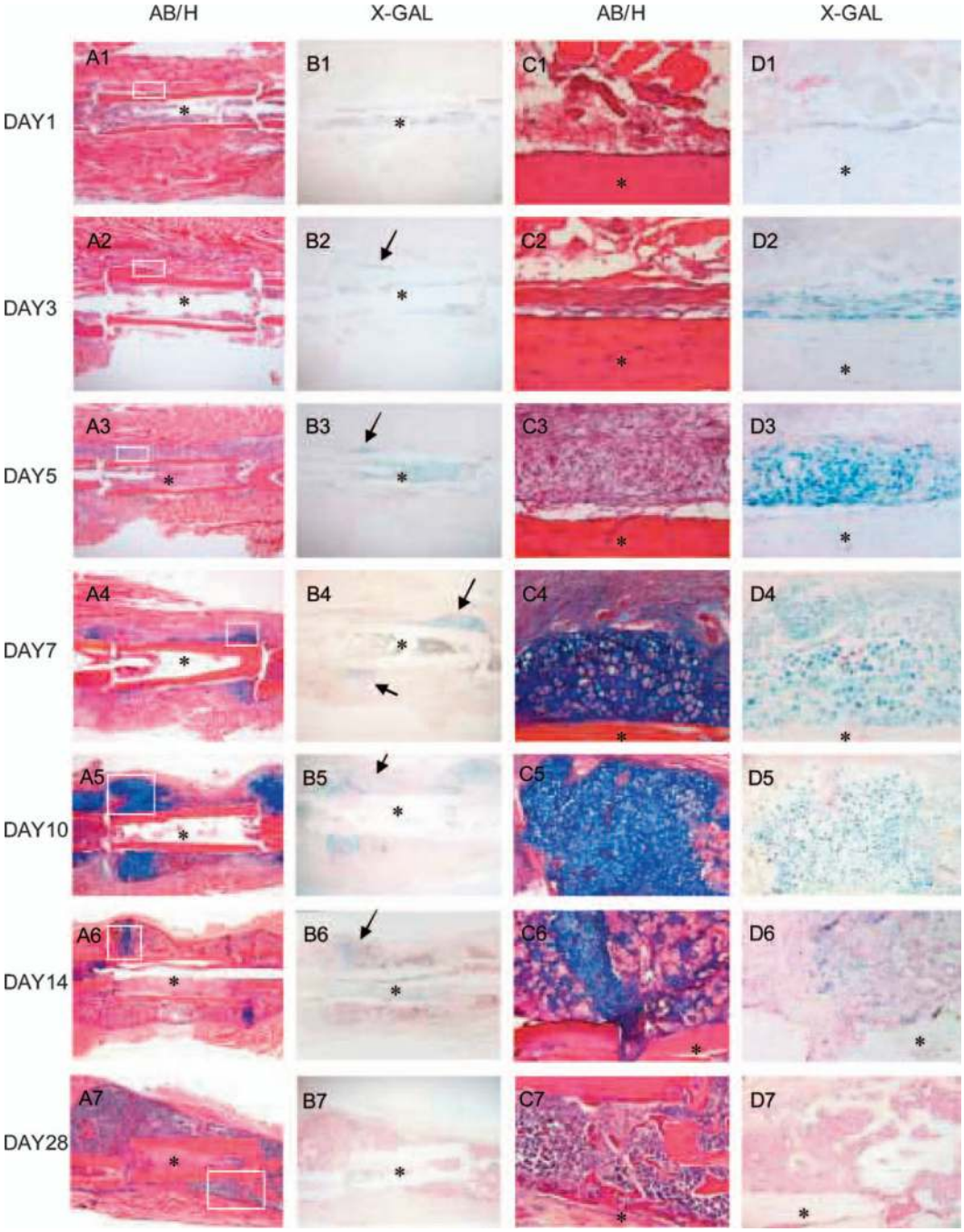

FIG. 2.

Progression of donor periosteal progenitor cell fate in endochondral bone repair. Live isografts (*) harvested from Rosa 26A mice were implanted in segmental defects in wildtype mouse femurs. Alcian blue/hematoxylin (A1–A7 and C1–C7) and X-gal staining (B1–B7 and D1–D7) were performed on relatively successive histologic sections obtained from the grafted femurs at days 1, 3, 5, 7, 10, 14, and 28 after grafting. Donor cells positive for β-gal (blue) were localized on the surface of the grafts (arrows) and in bone marrow. Boxed region in A is shown at higher magnification (×20) in C and D for Alcian blue/hematoxylin

and X-gal staining, respectively. The progression of donor periosteal progenitor cells (blue) fate through the endochondral bone formation pathway from day 1 to day 28 (D1–D7) is shown.

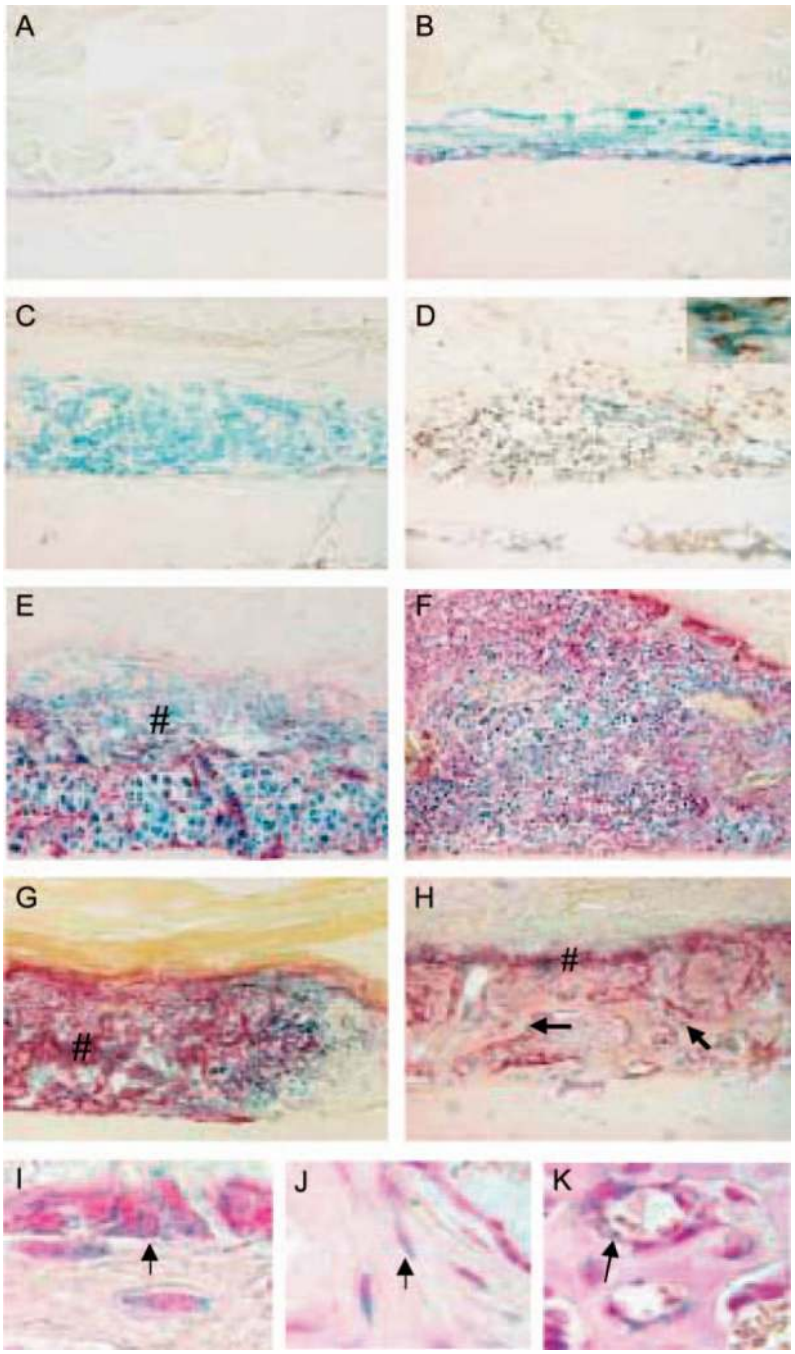

FIG. 3.

Characterization of donor periosteal progenitor cell differentiation. (A–C, E, and F) Double staining for β-gal and alkaline phosphatase were performed on histological sections obtained from the grafted femurs at days (A) 1, (B) 3, (C) 5, (E) 7, and (F) 10. BrdU labeling combined with β-gal staining was used to examine the proliferation of the early progenitor cells at day 5 (D, higher magnification for inset). (G) Donor progenitor cells underwent differentiation to form trabecular-like structures in the midshaft of the bone graft at day 7, with strong expression of alkaline phosphatase (#). (H) On day 10, more mature woven bone

was found with large numbers of β-gal–positive cells embedded in the new woven bone (arrows) and osteoblasts expressing high levels of alkaline phosphatase. Donor mesenchymal cell derived osteoblasts (arrow in I), osteocytes (arrow in J), and blood vessel lining cells (arrow in K) are shown at high magnification (×100).

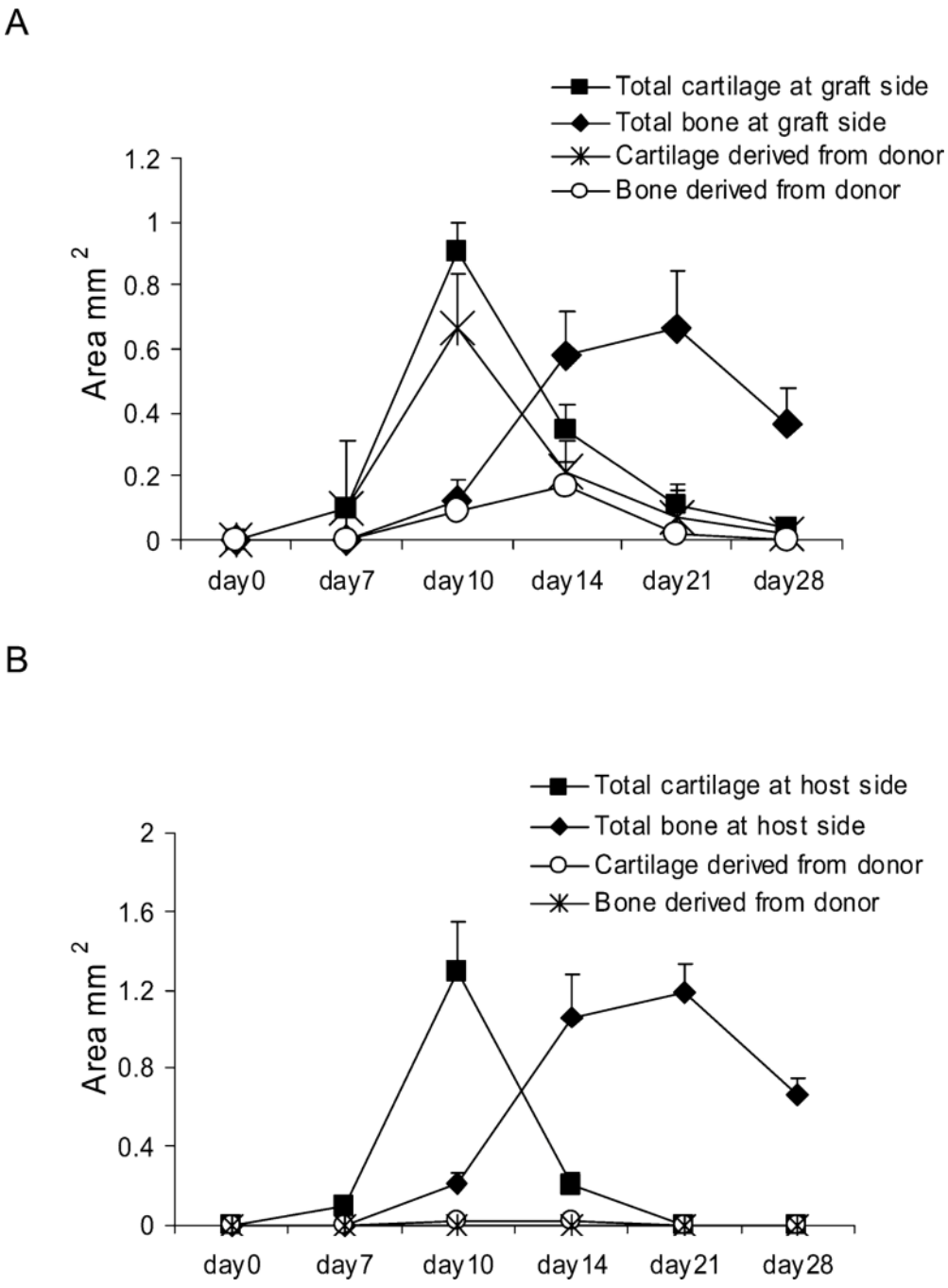

FIG. 4.

Histomorphometric quantification of donor cell contribution to osteogenesis in live isograft healing. Live donor isografts were harvested from Rosa 26A mice and implanted into their wildtype littermates. Femur sections stained for β-gal were used to perform quantitative histomorphometric analyses. A line was drawn at the cortical junction to separate the graft from the host. Areas of β-gal–positive (from graft) or –negative (from host) bone and cartilage were measured by computer tracing. Bone or cartilage formation on the surface of (A) the graft or of (B) the host bone was quantified separately. Three longitudinal tissue

sections of the femur from each animal were analyzed. Data shown represent mean ± SE values from five mice per group.

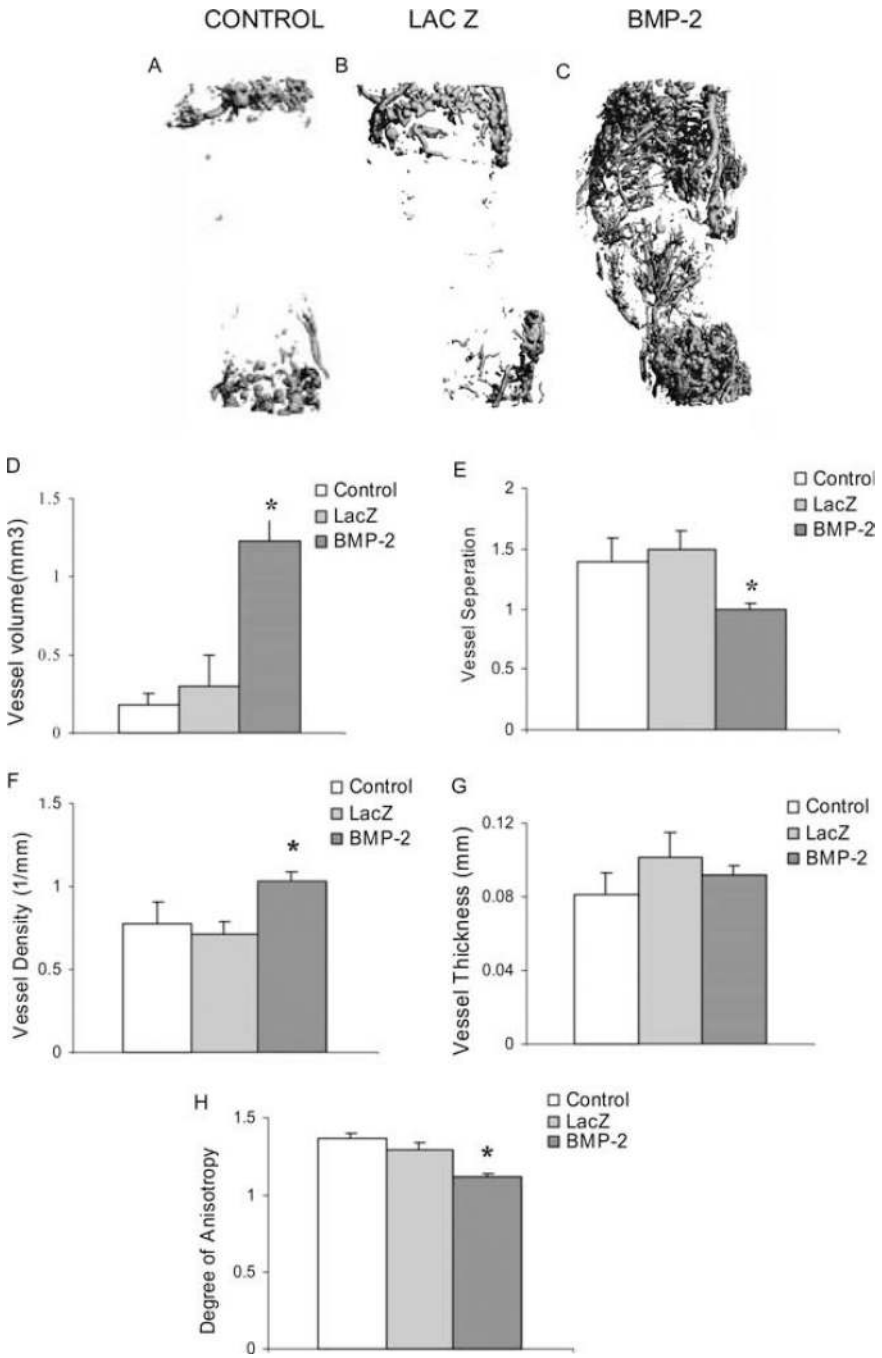

FIG. 5.

Marked induction of neovascularization in bone allografts implanted with BMP-2–producing BMSCs. Representative 3D vascular images of (A) allografts implanted with the scaffold alone (alloacellular) or with (B) bone marrow stromal cells infected by Ad-LacZ (allo-LacZ) or (C) Ad-BMP-2 (allo-BMP-2) 4 weeks after grafting. Quantitative analyses of vascular networks are shown as mean ± SE in (D) vessel volume, (E) vessel separation, (F) vessel density, (G) vessel thickness, and (H) degree of anisotropy. *$p < 0.05$, $n = 4$.

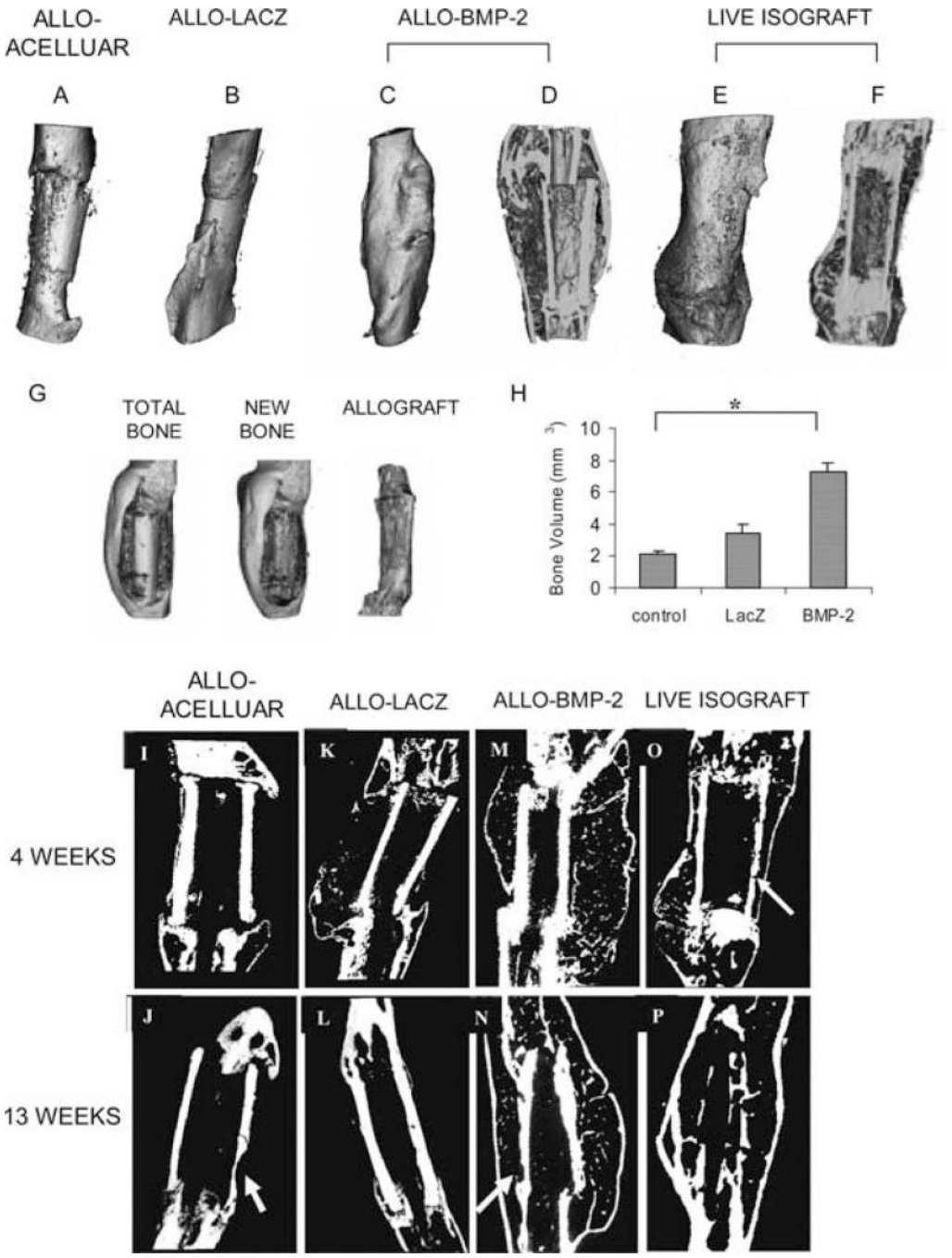

FIG. 6.

Formation of bridging new bone callus in allograft implanted with BMP-2–producing BMSCs. Graft healing and incorporation were examined by μCT analyses at 9 weeks after surgery. (A) Control allografts with scaffold only (allo-acellular), (B) allograft implanted with adenovirus LacZinfected marrow stromal cells (allo-LacZ), and (C and D) bone allograft implanted with BMP-2–producing marrow stromal cells (allo-BMP2) are shown. (E and F) For comparison, live isograft at 4 weeks after grafting is also shown. (G) New bone volume was quantified by subtracting bone allograft and host old cortical bone at the

junctions from the total bone. (H) Volumetric quantification data (as defined in G; mean ± SE; $n = 4$; $*p < 0.05$). (I–P) Representative longitudinal 2D μCT radiographs at 4 and 13 weeks after surgery from (I and J) control allograft, (K and L) allograft implanted with Ad-LacZ–infected cells, (M and N) allograft implanted with Ad-BMP-2–transduced cells, and (O and P) live isograft are shown. Arrows point to the areas of resorption on the grafts.

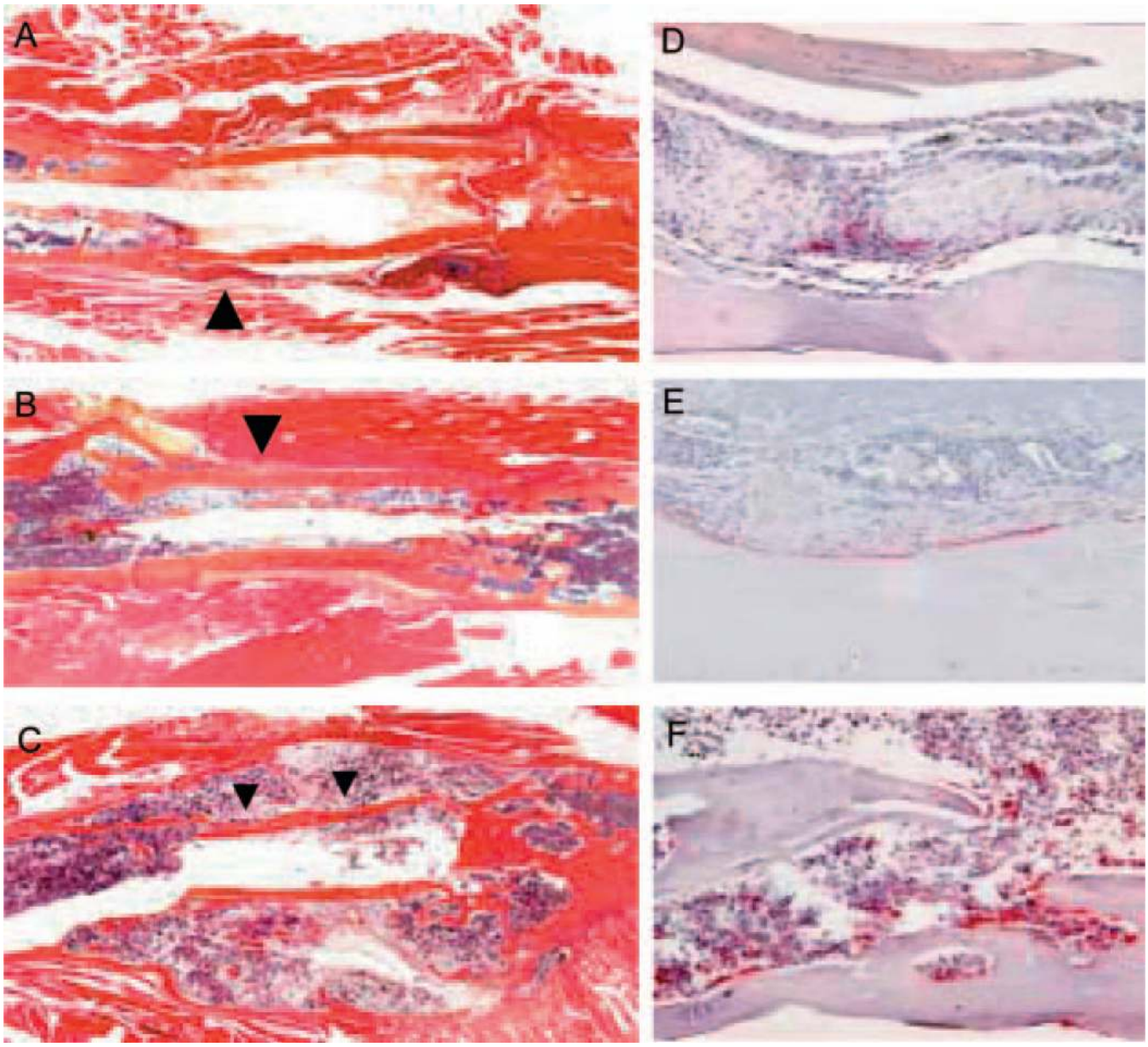

FIG. 7.

Comparison of allograft incorporation and resorption by histology. Representative H&E longitudinal sections from (A) control allograft (allo-acellular), (B) allograft wrapped with LacZ-infected cells (allo-LacZ), and (C) allograft implanted with BMP-2–producing cells (allo-BMP-2) 13 weeks after surgery are shown (×2). Arrows point to the site of resorption on the allografts. TRACP staining at higher magnification (×20) showed graft resorption in (D) control allografts, (E) LacZ-infected allografts, and (F) BMP-2/stromal cell–treated bone allografts.

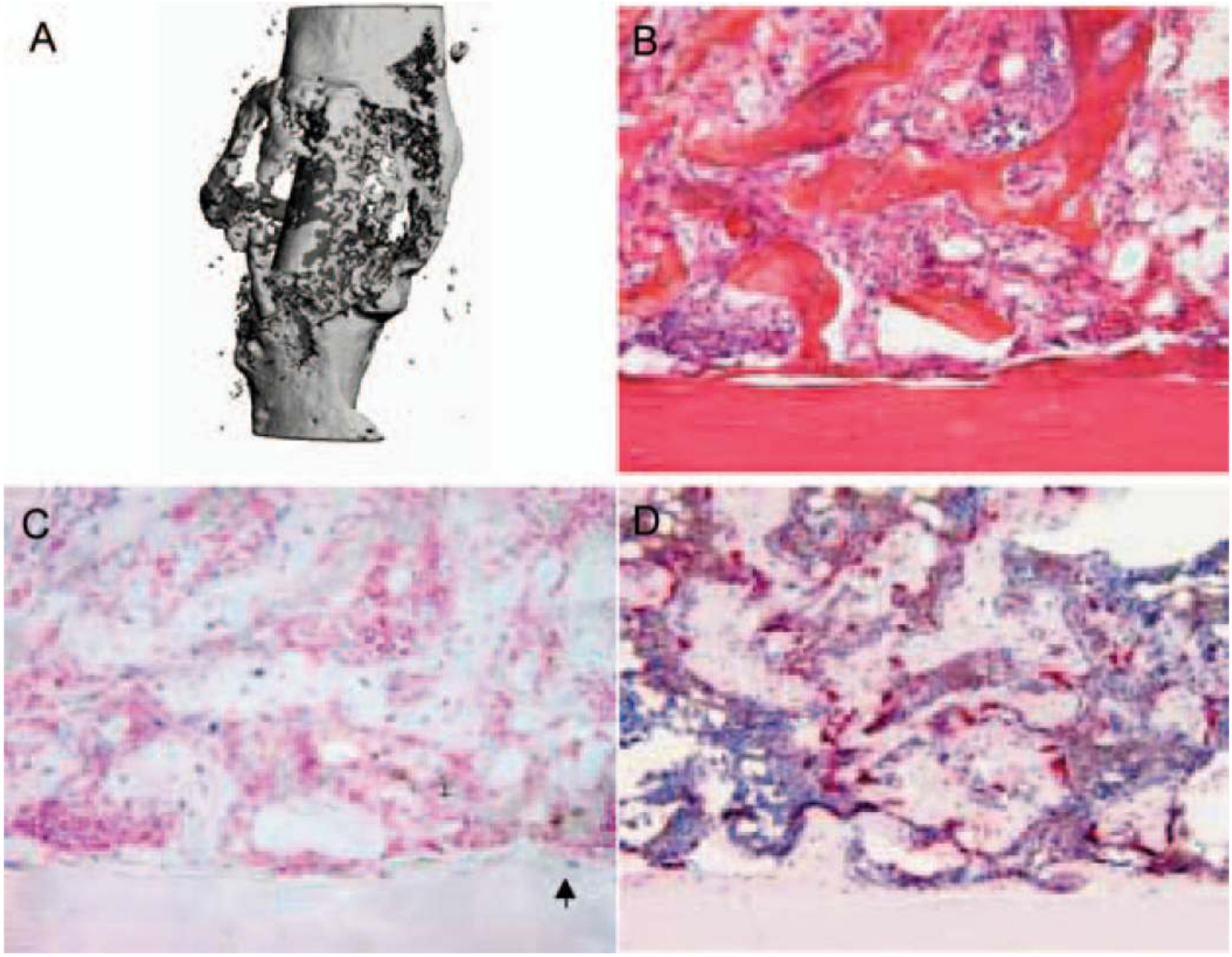

FIG. 8.

μCT imaging and histology of allografts treated with noninfected bone marrow stromal cells. About 5×10^6 bone marrow stromal cells harvested from Rosa 26A mice were seeded onto Gelfoam scaffolds and implanted onto allografts. (A) μCT imaging shows vigorous bone formation around the allograft 5 weeks after grafting. (B) H&E staining shows direct induction of new woven bone formation on the allograft surface. (C) X-gal staining shows the integration of blue donor osteocytes into new bone matrix (arrow), and (D) TRACP staining shows the recruitment of active osteoclasts to the graft.